Constraints on rigid zones and other distinct layers at the top of the outer core using CMB underside reflected PKKP waves[*]

Fenglin Niu[1,♦]   Cindi Kelly[1]   and   Jianping Huang[1,2]

[1] *Department of Earth Science, Rice University, Houston, TX 77005, USA*
[2] *School of Geosciences, China University of Petroleum, Qingdao 266555, China*

Abstract   Clear PKKP, a P wave reflects off the core-mantle boundary on the core side, is recorded by the transcontinental USArray from two deep earthquakes occurred in South America and Tonga, and one intermediate-depth earthquake in the Hindu Kush region. We compare the PKKP waveforms with the direct P waves to investigate the fine structures near the core-mantle boundary, with a primary focus on the core side. We find no evidence for the existence of a sedimentary layer of lighter elements with a thickness above a few hundreds of meters beneath the reflection points of the two deep events, which are located at the Ninety-East Ridge and South Africa. On the other hand the PKKP wave duration of the Hindu Kush event is almost twice as long as that of the P wave, suggesting that multiple reflections may be occurring at the core-mantle boundary located beneath the Antarctic, which is located inside the so-called tangent cylinder of the outer core. The tangent cylinder is an imaginary cylindrical region suggested by geodynamics studies, which has different flow pattern and may have a higher concentration in lighter elements as compared to the rest of the outer core. One possible explanation of the elongated PKKP is a thin distinct layer with a thickness of a few kilometers at the top of the outer core, suggesting that precipitation of lighter elements may occur at the core-mantle boundary. Our data also indicate an extremely low Q_P of 312, approximately 40% of the PREM average ($\sim$780), within the large-scale low-velocity anomaly in the lowermost mantle beneath Pacific.

Key words: PKKP; underside reflection; rigid zones under CMB; USArray
CLC number: P315.3   **Document code**: A

1 Introduction

Although it constitutes only $\sim$0.7% of the Earth's volume, the Earth's inner core plays a very important role in controlling the composition and dynamics of the outer core. The Earth's outer core is composed primarily of iron mixed with 10+wt% of lighter elements. Since lighter elements prefer to stay in the liquid side during the crystallization of the inner core, the concentration of lighter elements increases progressively since the formation of the inner core approximately 1 billion years ago (Labrosse et al., 2001). The exact age of the inner core is still a subject of active research. It is generally believed that the lighter elements and latent heat released during the iron solidification are the driving forces of the vigorous convection inside the outer core. The outer core is normally considered to be well mixed by this convection, and therefore is seismically homogeneous (e.g., Stevenson, 1987). Helffrich and Kaneshima (2004) found no seismic evidence for sharp density boundaries within the outer core that can be caused by immiscibility of the liquid Fe-O-S system.

Due to the presence of the inner core, there exhibit two distinct convection domains inside the outer core. Flow within the so-called tangent cylinder, a cylindrical region parallel to Earth's spin axis and enclosing the inner core (Figure 1a), seems to be relatively independent from the rest part of the outer core. Laboratory experiments conducted by Aurnou et al. (2003) suggest

that there is a little exchange in material between the tangent cylinder and its outside, and that the tangent cylinder can act as the reservoir of the lighter elements released from the solidification of the inner core. This implies that the tangent cylinder has higher concentration in lighter elements than the outside of it.

Rost and Revenaugh (2001) found a core rigid zone (CRZ), which has a small S-wave velocity of ∼0.7 km/s, at the top of the outer core beneath the southwest Pacific and they interpreted it as the sediments of lighter elements. Buffett et al. (2000) suggested that the liquid core should maintain a chemical equilibrium with the silicate mantle. Such an equilibrium could be disrupted by the progressive enrichment of the lighter elements inside the outer core during the solidification, leading to the precipitation of the lighter elements under the base of the mantle. Under such a scenario, it is more likely to

find core rigid zones and other distinct layers under the core-mantle boundary (CMB) inside the tangent cylinder.

While upperside reflection waves at the CMB, such as PcP and ScP, serve as a way to investigate fine seismic structures at both sides of the boundary (Rost and Revenaugh, 2001), underside reflections provide another means to detect distinct layers at the uppermost of the core. In this study we use PKKP, a seismic wave that enters the core, reflects at the CMB one time, propagates back to the surface through the CMB (Figure 1a). To examine the resolution of PKKP on fine scale seismic structures at the top of the outer core, we compute synthetic seismograms (Figure 1b) for various CRZ models using the Thomson-Haskell matrix propagator method (Haskell, 1962). Assuming a 1.5 km thick CRZ with a 1% change in P-wave velocity or in density,
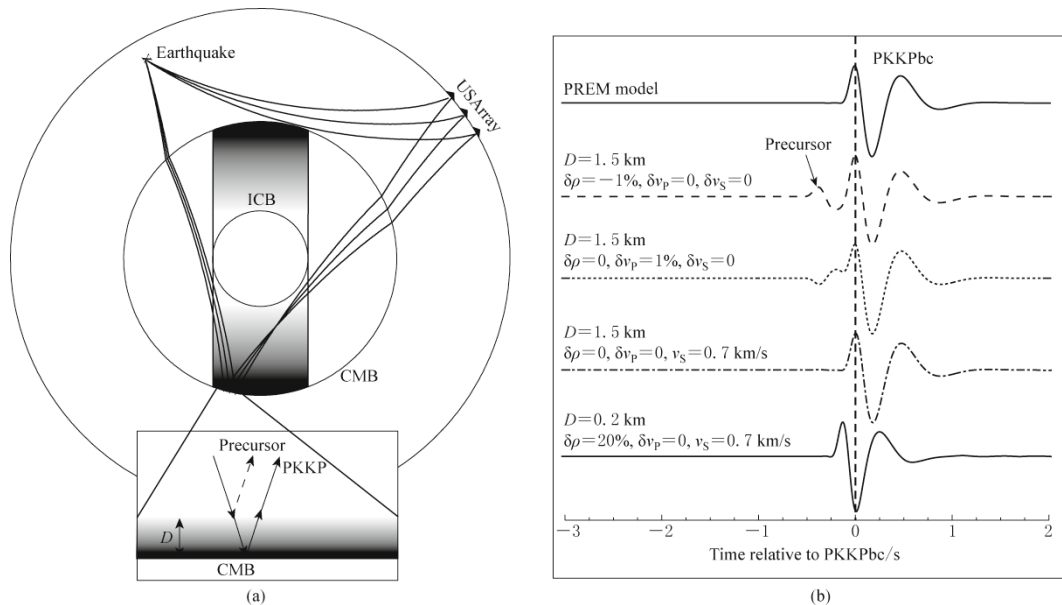
Figure 1 (a) Ray paths of the PKKPbc and the direct P waves at epicentral distances of 75°, 80°, and 85°. Inset shows possible reflections and reverberations when a distinct layer is present at the top of the outer core. (b) Thomson-Haskell synthetic seismograms for varying outer-core models with a distinct thin layer lying below the CMB. Three parameters are kept constant while one is varied: the dashed line stands for a 1.5 km layer with a 1% reduced density; the dotted line for a 1.5 km layer with a 1% increase of P-wave velocity; the dash-dotted line for a 1.5 km mushy layer with an S-wave velocity of 0.7 km/s; and the solid line for a thin CRZ proposed by Rost and Revenaugh (2001). Here the polarity of the CRZ waveform is reversed. We also show the PREM synthetic waveform in the top of the panel for comparison. Epicentral distance for the synthetics is chosen to be 80° and a source depth of 500 km is assumed. The synthetics indicate that the PKKP waveforms are very sensitive to velocity and density structure at the top of the outer core. We compare the waveforms of the PKKPbc and P to examine the pre- and post arrivals that might arise from structures at the top of the outer core. As waveforms are affected by many other elements such as attenuation, source directivity, we seek only robust difference between the two waveforms with different stacking methods.

we find a noticeable arrival prior to the PKKP phase (2nd and 3rd traces in Figure 1b). The P-wave reflection, on the other hand, appears to be less sensitive to S-wave changes (4th trace in Figure 1b). For a 200-m thick CRZ with an S-wave velocity of 0.7 km/s and a 20% reduced density, we find that the precursor becomes the dominant signal and that the main PKKP phase switches from positive to negative (the bottom trace in Figure 1b). The synthetics here indicate that PKKP and its precursory signals are very sensitive to outer-core structure below the CMB due to the high frequency nature of the P waves. In this study we compile a high-quality dataset of PKKP and P waveform from two deep-focus earthquakes and one intermediate-depth earthquake. We then compare the PKKP and P waveforms of each earthquake to identify signals prior to the PKKP arrival. As the three different earthquakes occurred in three different regions and their PKKP waves sample different parts of the outer core, we further investigate the lateral variations in the outer-core structure, especially the difference between the tangent cylinder and the rest part of the outer core.

2 Data and analysis

The seismic data used in this study are recorded by the USArray, which consists of 400+ transportable broadband seismic stations. Although the primary goal of the USArray deployment is to obtain high-resolution seismic images of the North American lithosphere, with an aperture of more than 2 000 km by 1 000 km, the USArray is also ideally suited for detecting anomalous signals associated with small-scale structures within Earth's deep interior around the world. Massive deployment of the transcontinental USArray started in 2005. We have searched the USArray recordings of intermediate-depth and deep-focus earthquakes occurring between 2005 and 2007 and found three events that show clear PKKP phases. The three earthquakes occurred in Hindu Kush, South America, Tonga regions (Table 1) and their PKKP reflection points are located beneath Antarctic, the Ninety-East Ridge, and South Africa, respectively (Figure 2). The former falls inside the tangent cylinder region and the latter two are located outside the tangent cylinder, thus a comparison

Table 1   Hypocentral information for events used in analysis

| Date	Time	Lat.	Long.	Depth/km	M_W	Region
2006-09-22	02:32:25.64	26.868°S	63.149°W	598	6.0	South America
2007-05-06	21:11:52.50	19.401°S	179.354°W	676	6.4	Tonga
2007-04-03	03:35:07.28	36.451°N	70.688°E	222	6.2	Hindu Kush
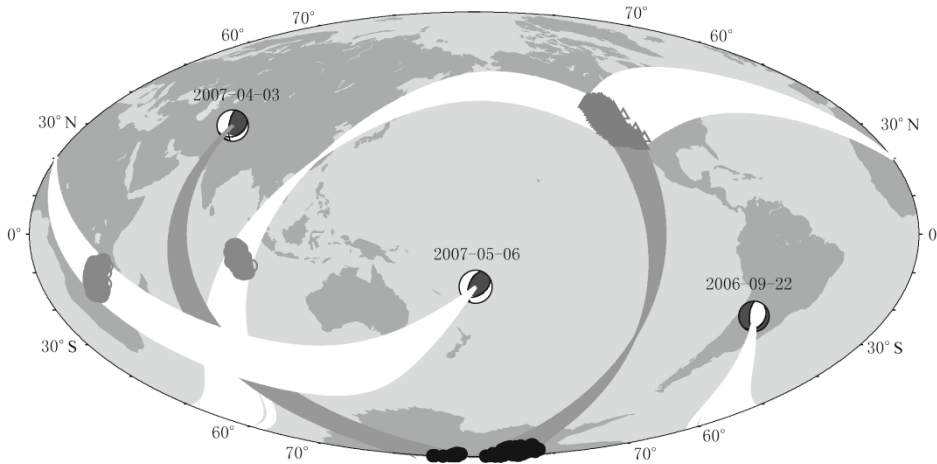
Figure 2   Map showing the locations of three earthquakes (beach balls) whose PKKPbc waves were clearly recorded by more than 200 USArray stations (grey triangle). Ray paths of the PKKP waves traveling along the major arc of the great circles are shown in white and gray lines. Reflection points at the core-mantle boundary are shown in grey circles. The PKKP waves from the Hindu Kush event (2007-04-03) reflect beneath the Antarctica (black solid circles) and sample the uppermost outer core located within the tangent cylinder, while those from the two deep events in South America and Tonga sample equatorial areas.

of the two groups offers new insights and constraints on whether the two convection domains inside the outer core have very different concentration in lighter elements, as well as dynamic processes beneath the CMB.

We begin our presentation by showing the PKKP waveforms of the three events recorded by the USArray (Figure 3). Here the broadband seismograms are first processed by a deconvolution of instrument response, and then a convolution with the WWSSN (WorldWide Standardized Seismograph Network) short-period in-

strument response. Data of the Tonga and the Hindu Kush events are further bandpass filtered between 0.5–1.6 Hz and 0.4–1.2 Hz, respectively, in order to get the best signal-to-noise ratio (SNR). The seismograms are subsequently aligned along either the first peak or the first trough. We only choose the seismograms with a SNR>5 for the final stacking and comparison analysis. This selection reduces the number of records from ∼200–400 to ∼30–50 for each event.
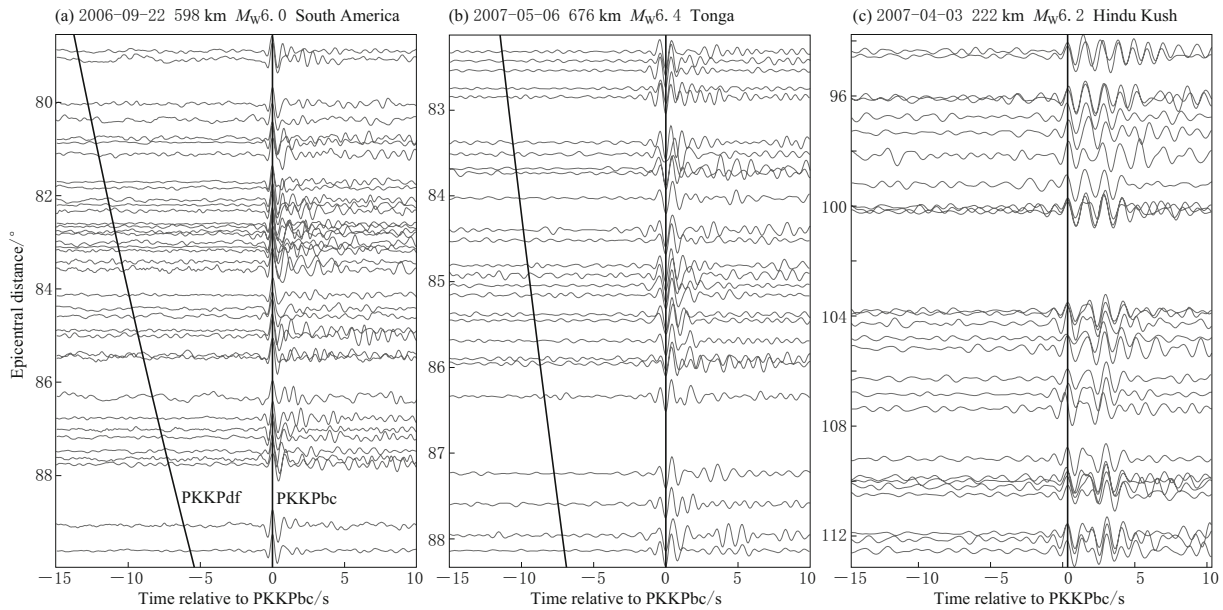
Figure 3 Vertical component of the USArray recordings. The broadband data are processed first with a deconvolution of instrument response, and then a convolution with the WWSSN (WorldWide Standardized Seismograph Network) short-period instrument response. Data of the Tonga (b) and the Hindu Kush events (c) are further bandpass filtered between 0.5–1.6 Hz and 0.4–1.2 Hz, respectively, in order to get the best signal-to-noise ratio (SNR). Seismograms are aligned according to the PKKPbc arrivals. Straight lines indicate PKKPdf arrivals predicted by the PREM model (Dziewonski and Anderson, 1981).

To make the comparison between PKKP and P waveforms robust and to enhance weak signals prior to the PKKP phase, we stack the individual waveforms. Two different stacking methods, the Nth-root stacking (Muirhead, 1968; Kanasewich, 1973) and the phase-weighted stacking (Schimmel and Paulssen, 1997), are employed. Both methods are designed to be more effective in enhancing coherent signals than the regular linear stacking method. Let $s_m(t)$ represents the amplitude at the mth aligned seismogram. The Nth-root and the phase weighted stack amplitude, $S_n(t)$ and $S_P(t)$, are given by

$$S_n(t) = a_n(t)|a_n(t)|^{N-1},$$

$$S_P(t) = \frac{1}{M}\sum_{m=1}^{M} s_m(t)\left|\frac{1}{M}\sum_{m=1}^{M}\exp\{i\phi_m(t)\}\right|^N, \quad (1)$$

where $a_n(t)$ is the Nth-root trace average, and $\phi_m(t)$ is the instantaneous phase. They can be calculated by the following equations:

$$a_n(t) = \frac{1}{M}\sum_{m=1}^{M}\text{sign}(s_m(t))|s_m(t)|^{1/N},$$

$$\phi_m(t) = \arctan\frac{H[s_m(t)]}{s_m(t)}, \quad (2)$$

here M is the total number of stations and $H[s_m(t)]$ is the Hilbert transform of $s_m(t)$. N is the power in-

dex of the Nth-root and phase weight stacking. When $N=1$, the Nth-root stacking becomes a regular linear averaging scheme. We have used both $N=1$ and $N=2$ in this study, and found that the choice of N has virtually no effect on our results. For the South America and Tonga events, we have stacked the same combination of stations to construct the P and PKKP waveforms for comparison. For the Hindu Kush event, we use 30 stations at epicentral distances between $94.4°$ and $112.5°$ to construct the PKKP waveform, and 30 stations between $94.1°$ and $96.1°$ to obtain the P waves since the

direct P wave disappears at around $97.8°$. As the PKKP and P waveforms show high similarity among different stations, we believe that the choice of different stations to construct P and PKKP wave does not affect the comparison.

3 Results and discussion

The stacked PKKP and P waveforms are shown in Figure 4. One common feature is that the PKKP waves always have higher frequency content than the direct P
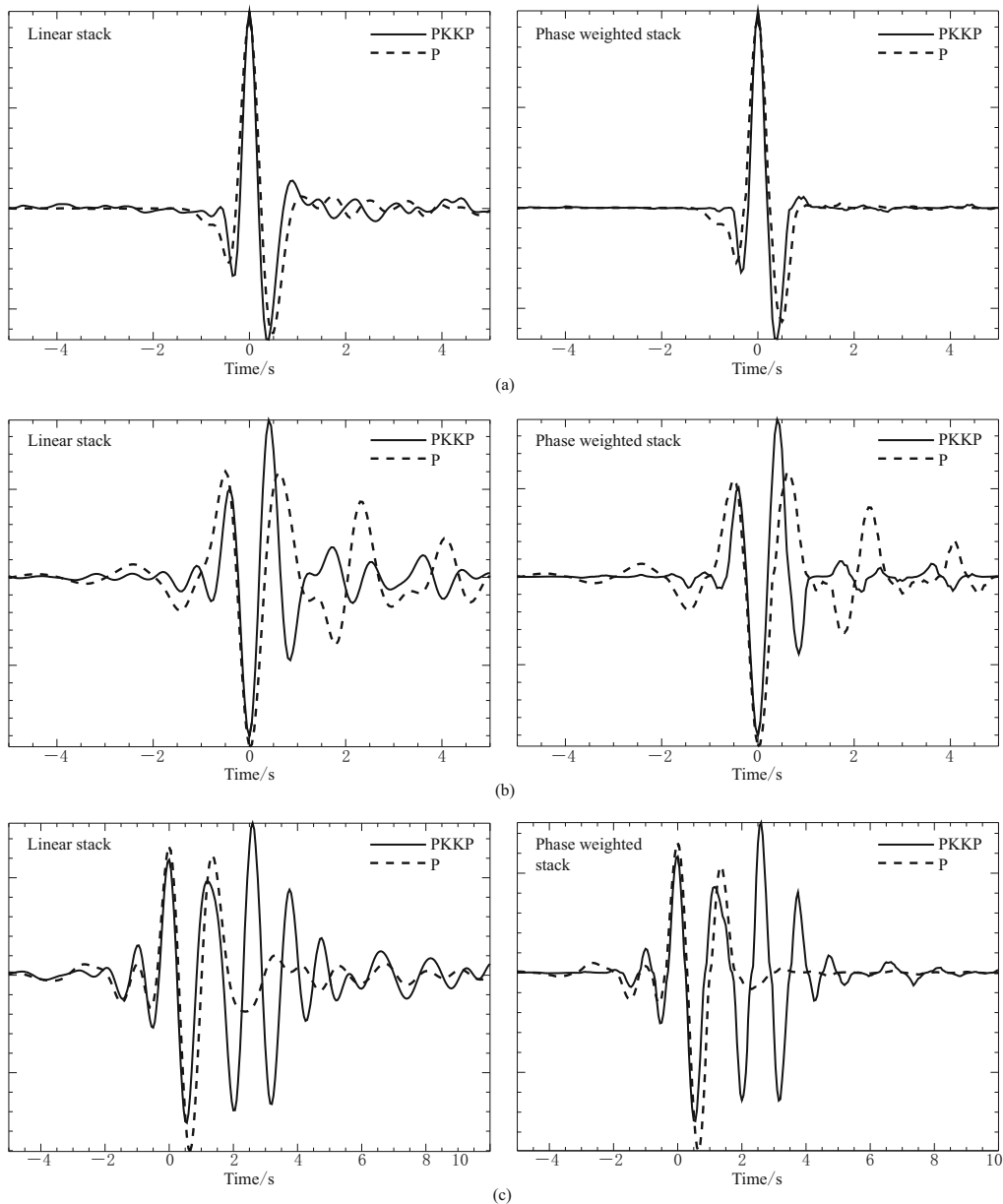
Figure 4 Stacked PKKPbc (solid line) and P (dashed line) waveforms of the South America (a), Tonga (b), and the Hindu Kush (c) events plotted together for comparison. Left panel are results of a linear stacking while those shown on the right side are derived from phase weighted stacking.

waves. This is expected based on the attenuation structure of the Earth. The PKKP waves have shorter ray paths in the mantle compared with the direct P wave and there is little attenuation inside the outer core. We measure the differential t-star (Δt^*),

$$\Delta t^* = \int_P \frac{1}{Q}\frac{\mathrm{d}l}{c(\omega_0)} - \int_{PKKP}\frac{1}{Q}\frac{\mathrm{d}l}{c(\omega_0)} \qquad (3)$$

by matching the attenuated PKKP waveforms with the direct P waves (Figure 5). Here Q and $c(\omega_0)$ are the quality factor and phase velocity at the reference angular frequency ω_0 (Aki and Richards, 2002; Oki et al., 2004). We take $\omega_0=2\pi$ in this study. We assume that the P and PKKP waveforms at the source are identical, and the observed difference in frequency is caused by physical dispersion related to the anelastic structure of the Earth. Thus we can synthesize a P waveform using the PKKP waveform under a certain differential Δt^* and differential traveltime Δt:

$$S_P(\omega) = S_{PKKP}(\omega)\times$$

$$\exp\left[\left(-\frac{1}{2}+\frac{\mathrm{i}}{\pi}\ln\frac{\omega}{\omega_0}\right)\omega\Delta t^* - \mathrm{i}\omega\Delta t(\omega_0)\right], \qquad (4)$$

here $S_P(\omega)$ and $S_{PKKP}(\omega)$ are the spectra of the P and PKKP waveforms, $s_P(t)$ and $s_{PKKP}(t)$, respectively. We use a grid search to find the Δt^* that gives the best match between the synthetic and the observed P waveforms. The estimated Δt^* from the South America, Tonga and the Hindu Kush events are 0.4, 1.5, and 0.7, respectively. The calculated Δt^* from the PREM Q model (Dziewonski and Anderson, 1981) is $\sim$0.4.

The high Δt^* value obtained from Tonga-USArray raypath suggests that the mantle ray segments of either the P waves or the PKKP waves have a very low or high Q values, respectively. We examine the P and PKP waveforms recorded at different azimuths and find that the large Δt^* is most likely associated with the lower mantle segments of the direct P waves between the Tonga and the USArray stations, which cross through the large low-shear-velocity province (LLSVP) in the lower mantle beneath central Pacific (e.g., Grand, 2002; Helmberger et al., 2005). In contrast, the PKKP ray paths from this event to the USArray stations sample the part of mantle with a rather normal seismic velocity. We thus attribute the observed $\Delta t^*=1.5$ to the attenuation structure along the lower mantle segments of the P-wave ray paths. With this assumption, we obtain an average Q_P of 312, approximately 40% of the averaged Q_P ($\sim$780) of the PREM model, suggesting that the LLSVP also has high attenuation structure.
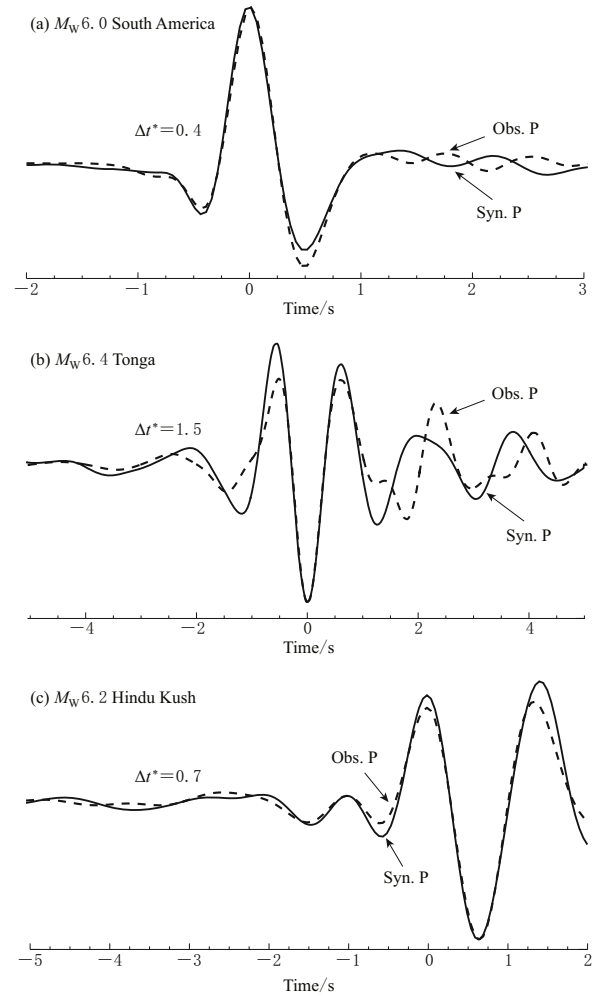
Figure 5 Synthetic (solid line) and observed (dashed line) P waveforms of the South America (a), Tonga (b), and the Hindu Kush (c) events plotted together for comparison. Synthetics are computed by convolving the PKKP waveform with the Δt^* operator shown in equation (4).

After the correction of attenuation, the PKKP and P waves of all the three earthquakes show high similarity with a cross correlation coefficient greater than 0.98 (Figure 5). Among the three events, the South American deep event has the simplest source time function and its PKKP phase shows the highest SNR. The PKKP and P waveforms are very similar, suggesting that there is no distinct structure in the outermost core beneath the Ninety-East Ridge (Figure 2). The Tonga earthquake has a slightly complicated source time function, but the PKKP and P match reasonably well once the large attenuation structure beneath central Pacific is taken into account. Thus it seems that the CMB structure beneath the PKKP reflection points, which are located beneath

South Africa (Figure 2), is also rather simple. There is no strong evidence for the presence of CRZs in these two regions. However, since the dominant frequency of the waveforms used in this study is around 1 Hz, it is essentially impossible for us to detect a thin layer of several hundreds of meters. The synthetic seismogram of the 200-m CRZ shown in Figure 1b is actually very similar to the PREM synthetics except for a ~0.1 s time shift and a polarity flip, which is far below the resolution of this study.

On the other hand, the PKKP waveform of the Hindu Kush event is almost twice as long as the P wave (Figure 4). We can only match the P waveform with the first part of the PKKP after attenuation being taken into account (Figure 5). In general, in addition to the attenuation structure, source directivity can also cause some difference between the P and PKKP waveforms, as the two waves leave the source with an azimuth 180° apart from each other. Specifically, the P and PKKP waves recorded by the USArray are radiated at an azimuthal direction of ~6° and ~186°, respectively. We thus chose the GEOSCOPE station RER at the Reunion island with an azimuth of ~196° and an epicentral distance of ~59° to examine directional variation in source time function. We notice that the P wave recorded at RER has a relatively larger takeoff angle (~32°) than the PKKP waves (~20°), and the radiating azimuths of two waves from the source are also slightly different (~10°), so the comparison may not be strictly desired. We find that the duration of the RER P wave is longer than those of the USArray records, but not enough to explain the nearly double duration of the USArray PKKP data.

We thus believe that the double arrivals observed here are related to structures near the CMB reflection points of the PKKP waves, which are located beneath the Antarctic, inside the tangent cylinder. Based on the calculated travel times of P and PKKP waves, the observed first arrival is closer to the PREM prediction. Therefore the most straightforward interpretation of the second arrival is some structure in the mantle side above the CMB. With this explanation, we find that a ~10 km thin layer with a P and S wave velocity drop in the range ~10% to 20% can explain the observed negative and large amplitude of the second arrival. However, the second arrival is only ~1–2 s away from the first one. Considering the uncertainty in source location and lateral heterogeneities in the mantle, it is not impossible that this second arrival is the main PKKP phase. In addition to the travel time, we also intend to use waveform

polarity to identify the PKKP phase. Both P and PKKP waves have a positive polarity when they are radiated from the source. Since the reflection coefficient at the CMB is negative, a π phase shift is added to the PKKP wave. In addition, the PKKP also experiences another π phase shift associated with the internal caustic at the antipode, respectively. After taking all the effects into account, the PKKP wave are expected to have the similar polarity to the P wave. The constraint on waveform polarity thus favors this interpretation. However, we are also aware that there is a large ambiguity in identifying waveform polarity with short-period data. If we assume that the second arrival is the main PKKP phase, then the first arrival must be caused by some boundary at the top of the outer core. Based on the observed ~1–2 s time difference, the thickness of the distinct layer could be as thick as 5–10 km. If this is the case, then it is probably a structure different from the thin CRZ observed by Rost and Revenaugh (2001) beneath the southwest Pacific. As indicated by the synthetic seismograms shown in Figure 1b, the PKKP precursor is very sensitive to density and P-wave velocity, not to S-wave velocity, structures within the distinct layer, thus the observed structure can be caused by a sharp density boundary resulting from liquid immiscibility, which was not observed by Helffrich and Kaneshima (2004) outside the tangent cylinder. We find that a 5-km distinct layer with a 5% density drop and a ~3% P-wave increase can explain the observed PKKP data.

There have been several seismic studies to determine whether the tangent cylinder is compositionally distinct from the rest of the outer core, as suggested by dynamic studies. Both body-wave (Yu et al., 2005) and normal-mode data (Ishii and Dziewonski, 2005) suggest that the overall perturbation of seismic velocity in the tangential cylinder is less than 0.1% as compared to the rest part of the outer core. High concentration of lighter elements within the tangent cylinder thus may occur only at the uppermost part of the outer core as the consequence of the buoyancy of the lighter elements.

4 Conclusions

We have analyzed hundreds of P and PKKP waveform data of one intermediate-depth and two-deep focus earthquake recorded by the transcontinental portable array in the United States to search for CRZs and other distinct structure in the top of the outer core. We find no evidence of anomalous layers thicker than a few hundreds of meters beneath two equatorial regions. On the

other hand, we find that the waveforms of the PKKP arrival, which reflects off the CMB beneath the Antarctic, extend as much as twice that of the P waves. The complicated PKKP waves can be interpreted by either an anomalous structure above the CMB or by a distinct thin layer with a thickness of <10 km at the uppermost part of the outer core inside the tangent cylinder. Previous studies have suggested that the difference in compressional wave speed and density between the tangent cylinder and the rest part of the outer core is <0.1%. Our results here thus may suggest that significant amount of sedimentation of the lighter elements may be occurring at the CMB within the tangent cylinder. Our data also suggest that the quality factor Q within the LLSVP is only ∼40% of the average value of the lower mantle, providing strong constraints on the origin of the large-scale low-velocity anomaly beneath the central Pacific.

References

Aki K and Richards P G (2002). *Quantitative Seismology.* 2nd ed. Herndon, Virginia, USA, 703pp.

Aurnou J, Andreadis S, Zhu L and Olson P (2003). Experiments on convection in Earth's core tangent cylinder. *Earth Planet Sci Lett* **212**: 119–134.

Buffett B A, Garnero E J and Jeanloz R (2000). Sediments at the top of Earth's core. *Science* **290**: 1 338–1 342.

Dziewonski A and Anderson D L (1981). Preliminary reference Earth model. *Phys Earth Planet Inter* **25**: 297–356.

Grand S P (2002). Mantle shear-wave tomography and the fate of subducted slabs. *Phil Trans R Soc A* **360**: 2 475–2 491.

Haskell N A (1962). Crustal reflections of the plane P and SV waves. *J Geophys Res* **67**: 4 751–4 767.

Helffrich G and Kaneshima S (2004). Seismological constraints on core composition from Fe-O-S liquid immiscibility. *Science* **306**: 2 239–2 242.

Helmberger D, Lay T, Ni S and Gurnis M (2005). Deep mantle structure and the postperovskite phase transition. *Proc Natl Acad Sci USA* **102**: 17 257–17 263.

Ishii M and Dziewonski A M (2005). Constraints on the outer-core tangent cylinder using normal-mode splitting measurements. *Geophys J Int* **162**: 787–792.

Kanasewich E R (1973). *Time Sequence Analysis in Geophysics.* Univ. of Alberta Press, Edmonton, AB, 364pp.

Labrosse S, Poirier J P and Le Mouel J L (2001). The age of the inner core. *Earth Planet Sci Lett* **190**: 111–123.

Muirhead K J (1968). Eliminating false alarms when detecting seismic events automatically. *Nature* **217**: 533–534.

Oki S, Fukao Y and Obayashi M (2004). Reference frequency of teleseismic body waves. *J Geophys Res* **109**: B04304, doi:10.1029/2003JB002821.

Rost S and Revenaugh J (2001). Seismic detection of rigid zones at the top of the core. *Science* **294**: 1 911–1 914.

Schimmel M and Paulssen H (1997). Noise reduction and detection of weak, coherent signals through phase-weighted stacks. *Geophys J Int* **130**: 497–505.

Stevenson D J (1987). Limits on lateral density and velocity variations in the Earth's outer core. *Geophys J R astr Soc* **88**: 311–319.

Yu W, Wen L and Niu F (2005). Seismic velocity structure in the Earth's outer core. *J Geophys Res* **110**: B02302, doi:10.1029/2003JB002928.